Structure *14*, 205–216, February 2006 DOI 10.1016/j.str.2005.10.014

Complete Reaction Cycle of a Cocaine Catalytic Antibody at Atomic Resolution

Xueyong Zhu,[1] Tobin J. Dickerson,[2,3] Claude J. Rogers,[2,3] Gunnar F. Kaufmann,[2,3] Jenny M. Mee,[2,3] Kathleen M. McKenzie,[2,3] Kim D. Janda,[2,3,4,*] and Ian A. Wilson[1,4,*]
[1]Department of Molecular Biology
[2]Department of Chemistry
[3]Department of Immunology
[4]The Skaggs Institute for Chemical Biology
The Scripps Research Institute
10550 North Torrey Pines Road
La Jolla, California 92037

Summary

Antibody 7A1 hydrolyzes cocaine to produce nonpsychoactive metabolites ecgonine methyl ester and benzoic acid. Crystal structures of 7A1 Fab′ and six complexes with substrate cocaine, the transition state analog, products ecgonine methyl ester and benzoic acid together and individually, as well as heptaethylene glycol have been analyzed at 1.5–2.3 Å resolution. Here, we present snapshots of the complete cycle of the cocaine hydrolytic reaction at atomic resolution. Significant structural rearrangements occur along the reaction pathway, but they are generally limited to the binding site, including the ligands themselves. Several interacting side chains either change their rotamers or alter their mobility to accommodate the different reaction steps. CDR loop movements (up to 2.3 Å) and substantial side chain rearrangements (up to 9 Å) alter the shape and size (~320–500 Å^3) of the antibody active site from "open" to "closed" to "open" for the substrate, transition state, and product states, respectively.

Introduction

Abuse of cocaine is a major public health concern and has been a significant societal problem (SAMHSA, 2004). Despite intensive multidisciplinary research, no effective treatments approved by the Food and Drug Administration (FDA) are available for cocaine craving, addiction, and overdose. The development of effective therapies for cocaine abuse has been frustrated by the difficulties inherent in inhibiting a blocking agent, since cocaine acts as an indirect dopamine agonist to block the dopamine transporter in the pleasure center of the brain. Nevertheless, a number of medications show some promise (Sofuoglu and Kosten, 2005). Immunopharmacotherapy has been proposed based on peripheral blockade rather than central blockade, in which antibodies are used to neutralize the drug, as a promising means to treat cocaine abuse (Carrera et al., 1995, 2000; Fox et al., 1996). Antibodies would intercept cocaine in the peripheral circulation before it is partitioned into the central nervous system, since the drug must pass through the blood to reach the brain.

Cocaine binding antibodies have shown promising effects to neutralize cocaine toxicity (Carrera et al., 2000); however, a limitation of the utility of cocaine binding antibodies is the 1:1 binding stoichiometry that would be saturated by larger doses of cocaine, whereas a catalytic antibody would be regenerated with each turnover. Administration of a monoclonal antibody (mAb) endowed not only with high binding affinity, but also with catalytic activity to metabolize cocaine, would have enhanced therapeutic effects if the kinetic properties of the antibody were appropriate (Matsushita et al., 2001).

Ester hydrolysis has been one of the hallmark reactions catalyzed by antibodies (Tanaka, 2002). Murine catalytic antibody 7A1 was elicited against a phosphonate mono-ester transition state analog (TSA) of cocaine **5** (GNL) (Figure 1) coupled through a covalent linkage to the carrier protein keyhole limpet hemocyanin (KLH) (Matsushita et al., 2001). Antibody 7A1 hydrolyzes the benzoyl ester of cocaine **1** to yield the nonpsychoactive metabolites ecgonine methyl ester **3** and benzoic acid **4** (Figure 1; Table 1). The potential therapeutic application for cocaine catalytic antibodies would be enhanced by improved kinetic parameters, manifested either by a lower K_M and/or by a greater k_{cat}. Thus, structural studies were initiated to determine the molecular basis for catalysis and to reveal possible mutations that could increase catalytic proficiency, as well as provide a foundation for the humanization of the murine antibody to facilitate human clinical trials.

Ideally, catalytic mechanistic studies should include experimentally determined structures of all steps along the reaction pathway, but that is rarely possible in practice. However, 7A1 Fab′ was amenable to cocrystallization with substrate, a transition state analog, and both products that enabled crystal structures of antibody 7A1 Fab′ as well as five complexes to be determined for the major steps along the reaction coordinate: the apo form, and complexs with substrate cocaine **1**, TSA **6**, both products (ecgonine methyl ester **3** and benzoate **4**), product ecgonine methyl ester **3**, and, finally, the other product, benzoate **4** (Table 2). 7A1 Fab′ in the heptaethylene glycol complex was also determined (Table 2) to probe antibody conformational flexibility. Here, we present snapshots of the complete cycle of the cocaine antibody catalytic reaction at atomic resolution.

Results

Activity Assay of Antibody 7A1

The kinetic parameters K_M, k_{cat}, and k_{uncat} for the hydrolysis of substrate cocaine **1** by mAb 7A1 were determined in three different buffer systems: 100 mM phosphate buffer (pH 7.4) with a K_M of 0.75 mM, a k_{cat} of 0.025 min^{-1}, and a k_{uncat} of 9.37 × 10^{-6} min^{-1}; 100 mM bicine buffer (pH 8.0) with a K_M of 3.47 mM, a k_{cat} of 0.087 min^{-1}, and a k_{uncat} of 2.93 × 10^{-5} min^{-1}; and 100 mM MOPS buffer (pH 7.4) with a K_M of 2.77 mM, a k_{cat} of 0.035 min^{-1}, and a k_{uncat} of 7.65 × 10^{-6} min^{-1}

*Correspondence: kdjanda@scripps.edu (K.D.J.); wilson@scripps.edu (I.A.W.)

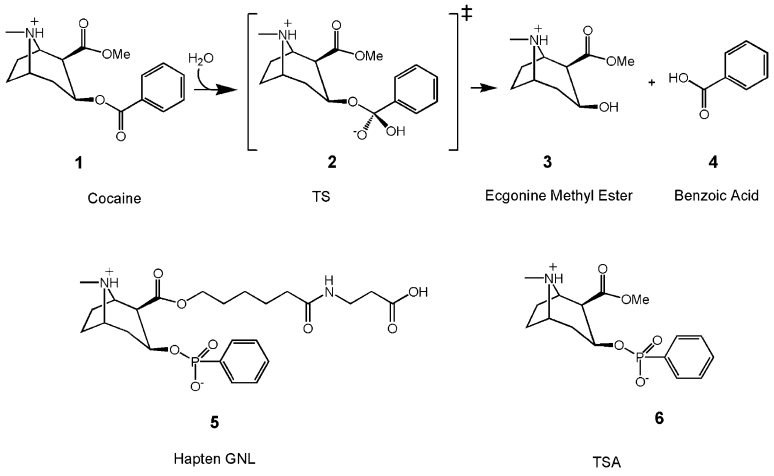

Figure 1. Antibody-Catalyzed Hydrolysis of Cocaine

Antibody 7A1 hydrolyzes cocaine **1** to give products ecgonine methyl ester **3** and benzoic acid **4** through transition state **2**. Hapten GNL **5** was used to elicit antibody 7A1, while transition state analog **6** was used in crystallization with 7A1 Fab′.

(Table 1). At measured pH values of 6.4, 7.1, 7.4, 8.0, and 8.5, the V_{max} of antibody 7A1 increased linearly with pH, with no rate enhancement over uncatalyzed rates below pH 6.4. Kinetic assays revealed no product inhibition in reactions containing benzoic acid up to concentrations of 10 mM, while slight inhibition was observed with ecgonine methyl ester at high concentrations ($IC_{50} \approx 5$ mM). Further, no inhibition of catalysis by heptaethylene glycol was detected up to 1 mM concentration. All of the experiments were performed three times, and the error bar for the measured K_M and k_{cat} values were less than or equal to 5% of the reported values.

Overview of the Crystal Structures

Seven structures of 7A1 Fab′ were determined at medium to high resolution (Table 2) in the apo form (1.5 Å) and as complexes with six ligands: substrate cocaine (1.5 Å); the transition state analog (1.85 Å); two products, ecgonine methyl ester and benzoic acid (2.1 Å); product ecgonine methyl ester (2.3 Å); product benzoic acid (1.85 Å); as well as heptaethylene glycol (1.70 Å). 7A1 Fab′ has an immunoglobulin (Ig) γ_1 heavy chain (H) and a κ light chain (L) (Figure 2). Electron density maps for all 7A1 Fab′ structures are of high quality, except for a flexible loop (residues 127–135) in the C_H1 domain, which usually has poor to no electron density in almost all Fab crystal structures (Zhu et al., 2003). The elbow angles between the variable and constant domains of the Fab molecules are 141.9° (apo form), 141.8° (substrate complex), 134.1° (TSA complex), 136.0° (two-product complex), 139.6° and 138.7° (ecgonine methyl ester complex for molecules **1** and **2**, respectively), 135.1° (benzoic acid complex), and 138.0° (heptaethylene glycol complex). The six complementarity-determining regions (CDRs) from the light (L1, L2, L3) and heavy (H1, H2, H3) chains that form the antibody-combining site have well-defined electron density and adopt known canonical conformations. CDR L3 resembles canonical structure 1 (Al-Lazikani et al., 1997) in the two-product complex, but, in the other structures, the backbone ϕ, ψ values of L95, L96, or L97 in CDR L3 deviate significantly from canonical mean values by 50°–100°. The torso of CDR H3 contains the characteristic β bulge at AspH101 (Morea et al., 1998), but the usual salt bridge between ArgH94 and AspH101 is not made due to steric block by TyrH102.

Table 1. Kinetic Parameters for Antibody 7A1-Catalyzed Cocaine Hydrolysis

Buffer	100 mM PB (pH 7.4)	100 mM Bicine (pH 8.0)	100 mM MOPS (pH 7.4)
K_M (mM)	0.75	3.47	2.77
k_{cat} (min^{-1})	0.025	0.087	0.035
k_{uncat} (min^{-1})	9.37×10^{-6}	2.93×10^{-5}	7.65×10^{-6}
k_{cat}/k_{uncat}	2.63×10^{3}	2.98×10^{3}	4.63×10^{3}

Architecture of the Antigen Binding Pocket

The bound ligands are all clearly visible in the electron density maps (Figure 3), allowing unequivocal identification of the catalytic pocket and the Fab-ligand interactions. The binding pocket is generally made up of aromatic residues; PheL91 (L3), PheL96 (L3), and AlaH34 (H1) constitute the floor of the pocket, while TyrL27D (L1), TyrL94 (L3), TyrH50 (H2), ArgH52 (H2), and TyrH97 (H3), as well as the main chain of ValL92 (L3) and GluL93 (L3), form the sides (Figure 3). The combining site pocket is a shallow groove rather than the deep pocket found in other esterolytic antibodies (Figures 3 and 4). In the 7A1 Fab′ apo structure at 1.5 Å (Figure 3A), the side chains of TyrL94 and TyrH97 have weak electron density, indicative of conformational flexibility, but they appear to be key for catalysis as suggested in the following 7A1 Fab′ substrate, TSA, and product complex structures. As in other antibody-hapten complexes (Wilson and Stanfield, 1993), CDR L2 does not contribute to the antigen-antibody interaction.

Substrate Binding

It is not common to crystallize enzyme-substrate complexes, but, in this case, a high concentration of cocaine (~20:1 molar ratio of cocaine to antibody Fab′) at pH 5.5 reduces the antibody activity and enables cocrystallization as a stable Michaelis-Menten complex (Figure 3B). Clear, interpretable electron density was found for cocaine in the active site with full occupancy, as reflected by the B values of the cocaine ligand (24–32 $Å^2$), which are comparable to nearby antibody residues (15–45 $Å^2$, average 24 $Å^2$). The cocaine molecule is buried such that the tropane moiety and the benzoate substituent

Table 2. Data Collection and Refinement Statistics of 7A1 Fab′ Crystals

Data Set	Native	Cocaine	Transition State Analog	Two Products[a]	Ecgonine Methyl Ester	Benzoic Acid	Heptaethylene Glycol
Space group	$C222_1$	$C222_1$	$P2_1$	$C222_1$	$P2_1$	$C222_1$	$P4_32_12$
Unit cell (Å)	a = 89.8, b = 117.3, c = 86.0	a = 90.3, b = 117.3, c = 85.2	a = 47.7, b = 73.7, c = 73.4	a = 83.6, b = 89.8, c = 154.4	a = 47.9, b = 78.5, c = 130.3	a = 82.6, b = 89.1, c = 153.5	a = 88.1, b = 88.1, c = 135.4
Unit cell (°)			β = 98.7		β = 91.9		
Resolution (Å)[b]	50.0–1.50 (1.55–1.50)	50.0–1.50 (1.54–1.50)	50.0–1.85 (1.92–1.85)	50.0–2.10 (2.15–2.10)	50.0–2.30 (2.38–2.30)	50.0–1.85 (1.89–1.85)	50.0–1.70 (1.76–1.70)
X-ray source	ALS 8.3.1	ALS 8.2.1	ALS 5.0.2	ALS 8.3.1	ALS 5.0.2	ALS 8.2.2	SSRL 9-2
Unique refs	72,464	72,094	40,762	34,262	40,412	48,913	59,095
Redundancy[b]	4.0 (3.1)	4.0 (3.0)	3.1 (3.0)	3.5 (3.0)	2.9 (2.0)	4.0 (3.5)	6.0 (5.5)
Average $I/\sigma(I)$[b]	35.4 (1.5)	41.6 (1.7)	24.0 (4.3)	23.8 (1.3)	20.3 (4.5)	31.7 (1.8)	36.2 (2.6)
Completeness[b]	99.5 (97.4)	99.5 (97.7)	94.7 (87.9)	99.3 (95.7)	90.2 (65.2)	99.6 (97.9)	99.8 (99.9)
R_{sym}[c]	0.038 (0.613)	0.052 (0.660)	0.066 (0.266)	0.074 (0.743)	0.099 (0.363)	0.058 (0.571)	0.057 (0.787)
Molecules in a.u.	1	1	1	1	2	1	1
V_{max} ($Å^3$/Da)	2.4	2.3	2.7	3.0	2.6	2.9	2.7
Refined residues	435	435	435	435	870	435	435
Refined waters	486	439	457	175	263	332	405
R_{cryst}[d]	0.181	0.182	0.227	0.225	0.238	0.217	0.209
R_{free}[e]	0.228	0.227	0.255	0.246	0.285	0.238	0.233
B values ($Å^2$)							
Protein	26.7	26.9	21.0	46.0	35.4	40.0	28.9
Water	41.0	39.2	34.9	52.9	40.7	51.4	40.1
Ligands	—	25.9	14.0	51.9	59.7	64.0	38.3
Ramachandran plot (%)[f]	90.2, 8.7, 0.5, 0.5	90.5, 8.4, 0.5, 0.5	90.2, 8.7, 0.5, 0.5	90.0, 9.0, 0.5, 0.5	88.9, 10.0, 0.8, 0.3	89.7, 9.5, 0.5, 0.3	90.0, 8.7, 0.8, 0.5
Rmsd bond (Å)	0.014	0.013	0.007	0.007	0.009	0.007	0.010
Rmsd angle (°)	1.6	1.6	1.4	1.4	1.6	1.4	1.3

[a] The two products are ecgonine methyl ester and benzoic acid.
[b] Parentheses denote outer-shell statistics.
[c] $R_{sym} = \sum_h\sum_i |I_i(h) - \langle I(h)\rangle| / \sum_h\sum_i I_i(h)$, where $\langle I(h)\rangle$ is the average intensity of i symmetry-related observations of reflections with Bragg index h.
[d] $R_{cryst} = \sum_{hkl} |F_o - F_c| / \sum_{hkl} |F_o|$, where F_o and F_c are the observed and calculated structure factors, respectively.
[e] R_{free} was calculated as for R_{cryst}, but on 5% of the data excluded before refinement.
[f] The values are a percentage of residues in the most favored, additional favored, generously allowed, and disallowed regions. MetL51, as expected, shows main chain torsion angles in the disallowed regions, but in a well-defined γ turn that is observed in most antibody structures (Al-Lazikani et al., 1997). SerH54, clearly defined in the electron density maps, also exhibits unusual main chain torsion angles at the tip of a γ turn.

lie on the floor of the binding pocket, with the carbonyl oxygen of the benzoyl ester pointing toward the outer rim of the cleft (Figures 3B and 4B). The cocaine adopts an energetically favorable chair conformation, and there is an intramolecular hydrogen bond between the tropane nitrogen and the carbonyl oxygen of the methyl ester, as observed in two cocaine binding antibodies (Larsen et al., 2001; Pozharski et al., 2005). Interestingly, this hydrogen bond is not observed in the small-molecule crystal structures of cocaine-HCl or its free

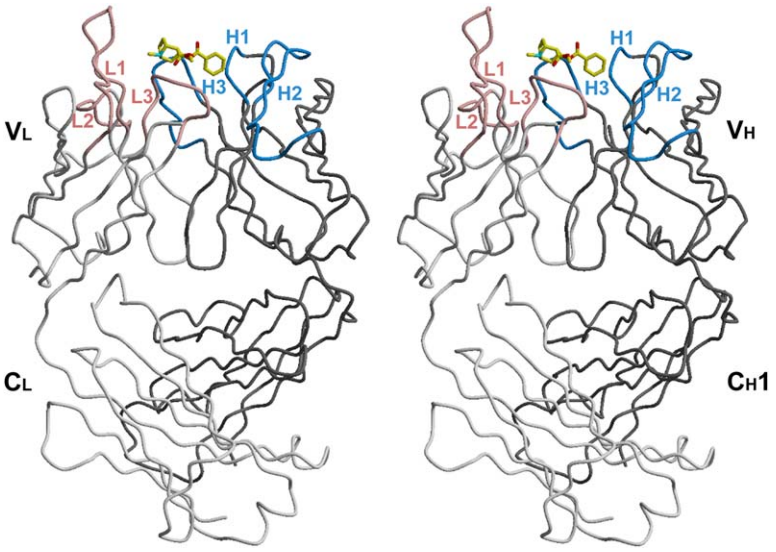

Figure 2. Crystal Structure of the 7A1 Fab′ Cocaine Complex with the C_α Trace of the Antibody Light and Heavy Chains Colored in Light and Dark Gray, Respectively

CDRs L1, L2, and L3 are colored brown, while CDRs H1, H2, and H3 are colored blue. Substrate cocaine is also shown with yellow carbons in the active site. All of the figures were generated in Bobscript (Esnouf, 1999) and rendered in Raster3D (Merritt and Murphy, 1994).

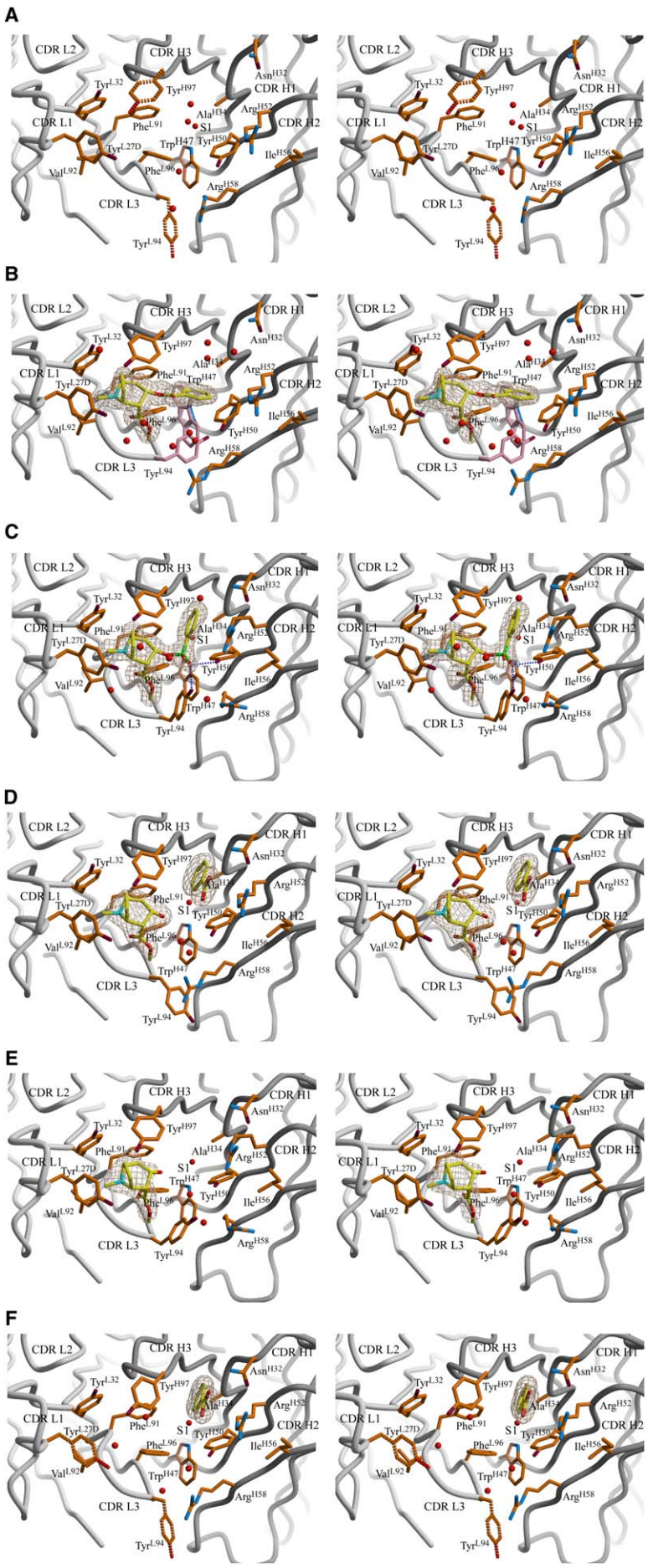

Figure 3. Stereoview of the Active Site of 7A1 Corresponding to Different Steps in the Reaction Pathway

(A) Apo form (1.5 Å).

(B) Complex with substrate cocaine (1.5 Å).

(C) Complex with the transition state analog (TSA) (1.85 Å).

(D) Complex with both products, ecgonine methyl ester and benzoate (2.1 Å).

(E) Complex with product ecgonine methyl ester (2.3 Å).

(F) Complex with product benzoate (1.85 Å). Disordered side chains are highlighted in dashed bonds. Alternate conformations of TrpH47 and the partially occupied TyrL94 are rendered with pink side chains in the 7A1 Fab′ cocaine complex. The corresponding ligands for each structure are shown with yellow carbons, blue nitrogens, red oxygens and green phosphorus atoms. Water molecules in the active site are shown in red spheres, and the conserved water is labeled S1.

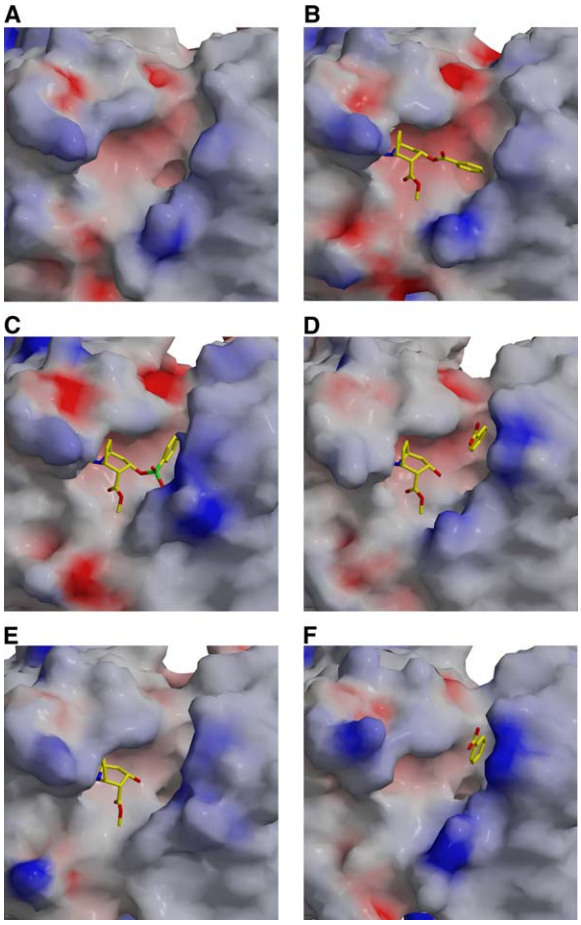

Figure 4. The Combining Site of 7A1 as It Changes Shape and Size throughout the Reaction Cycle

(A–F) The binding site is shown as a molecular surface colored by electrostatic potential (calculated with GRASP [Nicholls et al., 1991] with a 1.4 Å probe radius and contoured between −30 and +30 kT). The corresponding ligands are shown in ball-and-stick representation with yellow carbons. (A) Apo form. (B) Complex with substrate cocaine. (C) Complex with the transition state analog (TSA). (D) Complex with both products, ecgonine methyl ester and benzoate. (E) Complex with product ecgonine methyl ester. (F) Complex with product benzoate.

base, crack cocaine, from the Cambridge Structural Database (Allen, 2002). Cocaine-HCl was used in the cocrystallization, and the torsion angle around the methyl ester carbonyl (among O5-C6-C8-C10) is rotated about 120° in its complex with 7A1 Fab′, as compared to its small-molecule crystal structure. The tropane nitrogen atom to methyl oxygen distance is then reduced from 4.1 Å to 2.8 Å. The tropane nitrogen hydrogen in this intramolecular hydrogen bond also forms a bifurcated hydrogen bond with the main chain carbonyl oxygen of PheL91. Otherwise, the tropane and benzoate moieties are superimposable, with no obvious substrate strain on the cocaine molecule.

The cocaine molecule is 78% buried in the active site pocket (Figure 4B) that exhibits high complementarity to the ligand with a shape correlation parameter, Sc (Lawrence and Colman, 1993), of 0.89 (Table 3). A total of 74 van der Waals' interactions are made between the antibody and cocaine, 45 of which are derived from the light chain (Table 3). The majority of 7A1 Fab′ contact residues are hydrophobic or aromatic, with the exception of ArgH52. The tropane moiety contacts TyrL27D, TyrL32, PheL91, ValL92, and TyrH97; the methyl ester interacts with PheL91, ValL92, TyrL94, and PheL96; while the benzoate substituent contacts AlaH34, TyrH50, ArgH52, and PheL96. At physiological pH, the tertiary amino group of cocaine (pKa ~8.6) would be protonated, affording a net positive charge. Interestingly, the positively charged tropane nitrogen atom is centered almost exactly over the aromatic ring of TyrL27D and TyrL32, with distances of 4.6 and 4.3 Å between the nitrogen atom and the centers of the aromatic rings; these data are consistent with a cation-π interaction, as found in many proteins (Dougherty, 1996).

The cocaine scissile benzoyl ester carbonyl carbon, which should be the target of nucleophilic attack by a general base or hydroxide ion, is distant (at least 6 Å) from any likely active site candidates, and the closest water molecule is 3.9 Å. Thus, the Fab′ in the cocaine complex appears to be inactive or in a low activity form at this pH, consistent with lack of cleavage of the cocaine ligand. The apo antibody is also presumably in a catalytically inactive state and is complementary to neither substrate nor transition state. As the apo 7A1 Fab′ and cocaine complex crystallize in the same conditions with similar crystal packing, conformational changes can be accurately assessed between these two crystal structures. Both structures superimpose well, with an rmsd for all C_α atoms of the Fv domain of 0.32 Å, which corresponds to the approximate experimental error (~0.2 Å). For the CDR loops, the largest, but still relatively small, backbone differences are observed around LeuL27C–TyrL32 (rmsd of C_α atoms of 0.6 Å) of the L1 loop and PheL91–ProL95 (rmsd of C_α atoms of 0.7 Å) of L3, which slightly enlarge the combining site. The most significant conformational changes occur for TyrH97 and TyrL94 in the active site, which are flexible in the apo form; however, in the cocaine complex, TyrH97 is fully ordered, while TyrL94 has partial occupancy to accommodate alternate conformations of TrpH47.

Table 3. Protein-Ligand Interactions in Antibody 7A1

Data Set	Apo	Cocaine	Transition State Analog	Two Products[a]	Ecgonine Methyl Ester	Benzoic Acid	Heptaethylene Glycol
van der Waals contacts	n/a	74	98	79	43	25	57
H bonding	n/a	1	3	2	0	1	1
Volume of combining site (Å^3)	~500	~480	~320	~410	~400	~440	~370
Shape correlation (Sc)	n/a	0.89	0.87	0.81	0.84	0.76	0.73

[a] The two products are ecgonine methyl ester and benzoic acid.

Recognition of the Transition State Analog

Antibody 7A1 was raised against hapten **5**, which is a transition state analog containing a linker for covalent attachment to keyhole limpet hemocyanin for immunization. Several esterolytic antibodies have been raised against phosphonate haptens that mimic the putative tetrahedral transition state of the hydrolytic reaction. In the 7A1 Fab′ TSA complex (Figure 3C), the overall location and orientation of the tropane and methyl ester of the TSA with respect to the Fab′ is similar to that seen in the 7A1 cocaine complex, with 90% of its accessible surface being buried (Figure 4C) and high shape complementarity with an Sc of 0.87 (Table 3). As in the cocaine complex, an intramolecular hydrogen bond is formed between the tropane nitrogen atom and the carbonyl oxygen of the methyl ester, as well as a bifurcated hydrogen bond between the tropane nitrogen atom and the PheL91 carbonyl oxygen.

The contribution to catalysis of the differential stabilization of the transition state relative to substrate can be analyzed by comparing the 7A1 Fab′ interactions with the scissile carbonyl in the substrate versus the charged tetrahedral phosphonate in the TSA, as well as from the relative disposition of the tropane skeleton-methyl ester and phenyl ring moieties in both ligands. The tropane-methyl ester moiety of the TSA makes tight interactions with the same nine residues of the combining site in both structures, except for TyrL94, which adopts a different side chain rotamer that leads to a slight translocation of the tropane moiety by about 0.8 Å toward the center of the combining site. However, the phenyl ring changes dramatically from the substrate to TSA so as to stack between CDRs H3 and H1, H2. In the TSA complex, the phenyl ring interacts with TyrH97, AspH96, AlaH34, TyrH50, and ArgH52. The negatively charged pro-*R* phosphonyl oxygen of the TSA is within hydrogen bonding distance of TyrL94 (2.5 Å) and TyrH50 (2.6 Å), which both can act as hydrogen bond donors, while the pro-*S* oxygen points out toward solvent. We, therefore, propose that TyrL94 and TyrH50 constitute the oxyanion hole in 7A1 to stabilize the transition state.

The 7A1 Fab′ structures in the substrate and TSA complexes superimpose with an rmsd of C_α atoms of 0.64 Å. For the CDR loops, the most significant backbone shift is observed around ArgH52–ArgH58 (rmsd of 1.5 Å for C_α atoms) of CDR H2, and the largest movement (~2.3 Å) is seen for the C_α atom of ValH55. A small change occurs around LeuL27C–TyrL32 (rmsd of 0.6 Å for C_α atoms) of CDR L1. However, the most significant conformational changes occur for several active site residues that adopt different combinations of side chain rotamers and main chain movements; TyrL94 OH differs by 6.6 Å, TyrH50 OH differs by 2.6 Å, Arg52 C_ζ differs by 3.4 Å, and ArgH58 C_ζ differs by 5.4 Å. The active site compresses on TSA binding, and the total volume is reduced to ~320 $Å^3$ compared to 480 $Å^3$ in the cocaine complex (Table 3, calculated with GRASP [Nicholls et al., 1991]), mainly due to movement of CDRs H2 and L1 and side chain rotations of the aforementioned residues (Figures 4B and 4C).

Interactions of the Two Reaction Products with the Active Site

High concentrations of both products, ecgonine methyl ester (3.8 mM) and benzoic acid (3.8 mM), were used in the cocrystallization with 7A1 Fab′. Clear electron density (Figure 3D) was apparent for both ligands that are both 86% buried in the active site (Figure 4D). The ecgonine methyl ester superposes within experimental error (rmsd of 0.2 Å) with the corresponding moiety of the TSA (Figure 3C) and makes similar hydrogen bonds, cation-π interactions, and van der Waals' interactions; however, TyrL94 shows yet another side chain rotamer and partial occupancy. The benzoic acid rotates significantly compared to the benzoyl moiety of the TSA; thus, its carboxyl group points toward the solvent (Figure 3D). The benzoate carboxylate is almost parallel to the ArgH52 guanidinium, with a distance of about 3.8 Å, and it contributes to electrostatic interactions. The benzoic acid interacts with AsnH32, AlaH34, ArgH52, AspH96, and TyrH97 (21 van der Waals' contacts, one H bond with AsnH32), but not with TyrH50 as in the TSA complex. For the CDR loops, slight backbone shifts (Figures 3C and 3D) again arise around ArgH52–ArgH58 (rmsd of 0.6 Å for C_α atoms) of CDR H2, LeuL27C–TyrL32 (rmsd of 0.4 Å) of CDR L1, and PheL91–ProL95 (rmsd of 0.9 Å) of CDR L3. For active site residues, TyrL94 OH shifts by 8.7 Å, TyrH50 OH shifts by 1.3 Å, ArgH52 C_ζ shifts by 2.2 Å, and ArgH58 C_ζ shifts by 4.8 Å due to different side chain rotamers coupled to main chain movements. The resulting active site volume is ~410 $Å^3$, which is larger than the TSA complex (~320 $Å^3$), but smaller than the cocaine complex (~480 $Å^3$) (Table 3).

Interactions of Product Ecgonine Methyl Ester with the Active Site

As expected, the crystal structures of 7A1 Fab′ in complex with ecgonine methyl ester (Figure 3E) is very similar to its complex with both products (Figure 3D), with rms deviations for Fv equivalent C_α atoms of 0.4 Å, excluding the first 12 residues of the light chain (0.65 Å for residues 1–105 in both chains). Intriguingly, 7A1 Fab′ in complex with ecgonine methyl ester (Figure 3E) also superimposes closely with the TSA structure (Figure 3C) with an rmsd of 0.44 Å (Fv C_α), and the ecgonine methyl ester makes similar contacts to the Fab′ with 7 van der Waals' interactions with TyrH97 and 36 van der Waals' interactions with V_L. No hydrogen bonds are formed, as the tropane nitrogen atom is 3.8 Å from the carbonyl oxygen of PheL91; however, cation-π interactions are still made with TyrL27D and TyrL32. The CDR loop conformations are similar to those of the two-product complexes, as well as the active site residue rotamers, except, again, for TyrL94 and ArgH58, which rotate toward their conformation in the TSA complex. In this case, these two side chains might be influenced by crystal packing, as symmetry-related residues H162–H165 would collide with these residues if they adopted the same conformation in the two-product complex. Hence, TyrH94 is fully occupied and makes additional van der Waals' interactions with the methyl ester of the ligand.

Interactions of Product Benzoic Acid with the Active Site

The benzoic acid complex structure (Figure 3F) is also similar to that of the two-product complex, with an rmsd of 0.22 Å (Fv C_α). No significant conformational changes were observed, except for a slight shift of

CDR L3 (ValL92–PheL96, rmsd of 0.7 Å for C_α atoms). The benzoic acid occupies a similar position and makes 25 van der Waals' contacts with AsnH32, TyrH33, AlaH34, ArgH52, and TyrH97, and it makes 1 hydrogen bond with AsnH32 (Table 3). As with the two-product complex, the guanidinium of ArgH52 is almost parallel to the carboxylate group of benzoic acid at a distance of 3.8 Å, contributing to an electrostatic interaction. It is noteworthy that most active site residues retain the same side chain rotamers as in the two-product structure, except for TyrL94 which continues to be flexible. Interestingly, TyrL27D is now disordered compared to the other 7A1 Fab′ structures.

Discussion

Conformational Changes along the Reaction Coordinate

Understanding the molecular mechanism of protein catalysis and allosteric regulation has been a key focus of modern biochemistry and structural biology. The importance of isomerism and induced fit in enzyme catalysis has long been recognized; thus, protein flexibility is now known to be an essential characteristic of most enzymes. It is commonly accepted that, in most enzymes, the "open" form of an enzyme initially binds the substrate, and then closes around the substrate in the "closed" form. Catalysis takes place within the closed form, after which the enzyme including the active site loops opens to release the product. The catalytic and binding residues are often amongst the most flexible parts of the structure, although the overall structure may not change significantly; in some cases, large domain rearrangements are observed in multidomain proteins upon substrate binding (Gutteridge and Thornton, 2004).

Ideally, enzyme mechanistic studies should include experimentally determined structures of all of the steps along the reaction coordinate, but that is rarely possible in practice. This series of crystal structures of antibody 7A1 has provided snapshots for each of the six steps along the reaction coordinates (Figures 3 and 4). Significant conformational changes of up to 9 Å, especially for key residues, occur along the 7A1-catalyzed cocaine hydrolysis pathway and play a critical role in the catalytic reaction. In the unliganded apo structure, the active site adopts an "open" form, in which the side chains of two key residues, TyrL94 and TyrH97, are highly flexible (Figure 3A). When the antibody binds cocaine, the active site still retains a modified "open" form, in which TyrH97 now becomes fixed, TyrL94 displays some partial stabilization, and TrpH47 populates two side chain rotamers (Figure 3B). In the transition state, the active site adopts the "closed" form, in which the CDR loops, particularly H2, progress toward the active site (Figure 3C). TyrL94 and TyrH50 now rotate and shift to make hydrogen bonds with the pro-*R* phosphonate oxygen, and they generate an oxyanion hole to stabilize the transition state. The side chains of ArgH52, ArgH58, and IleH56 reposition themselves by several angstroms, thus contributing toward TSA sequestration within the active site that stabilizes the oxyanion intermediate more efficiently than the substrate. When cocaine hydrolysis is completed, the two products initially remain trapped in the active site that now returns to an intermediate "open" form; the side chains of TyrH50, ArgH52, ArgH58, and IleH56 adopt conformations between those found in the transition state and those in the substrate bound state, and the side chain of TyrL94 shows partial occupancy and a different rotamer (Figure 3D).

Protein conformational changes among different states of a catalytic reaction can be categorized into four different types of motions: side chain rotamer changes, loop movements, secondary structure changes, and domain motions (Gutteridge and Thornton, 2004). These changes enhance binding of substrate, optimally orientate the catalytic groups, remove water from the active site (except if catalytic), and trap and stabilize intermediates. In 7A1, only loop movements and side chain motions appear to play dominant roles in the cocaine hydrolysis reaction, but these alter the binding pocket volumes considerably (from ~320 to 500 $Å^3$) (Table 3). However, other small motions could still be important for catalysis, as residue movements of less than 1 Å can alter the rate of catalysis by several orders of magnitude (Koshland, 1998). Although static snapshots given by X-ray crystallography do not completely reveal the entire dynamics of the catalytic process, these crystal structures represent a clear view of the enzyme state at each stage in the reaction cycle.

The conformational flexibility of the 7A1 active site is further confirmed by the crystal structure of 7A1 complexed with heptaethylene glycol (Figure 5) from the crystallization solution. The active site pocket (Figure 5) is similar in size to that of the two-product complex (Figure 3E), in which TyrH50, ArgH58, ArgH52, and IleH56 superimpose well within experimental error, but TyrL94 and TyrH97 are fixed in rotamers not observed in the other 7A1 Fab′ structures. TyrL94 now points away from the active site center, while TyrH97 flips into the pocket that benzoic acid occupied in the product complexes, and its side chain hydroxyl oxygen forms a hydrogen bond with the carboxamide of AsnH32. To our knowledge, the binding of heptaethylene glycol to an antibody-combining site has not been reported before, although, here, it does not show any obvious inhibition of the 7A1 catalytic reaction.

Catalytic Mechanism

Direct hydroxide attack on the scissile carbonyl of the substrate is a likely mechanism for antibody-catalyzed esterolytic reactions and has been confirmed in crystal structures of esterolytic antibodies that were elicited by phosphonate haptens that mimic the transition states of the reaction (MacBeath and Hilvert, 1996). The mechanism of nonenzymatic hydrolysis of cocaine has been explored (Zhan and Landry, 2001), and calculations on methyl and benzoyl ester hydrolysis suggest that formation of a tetrahedral intermediate via hydroxide attack on the carbonyl carbon is the rate-determining step. In the 7A1-cocaine structure (Figure 3B), all residues that could potentially promote nucleophilic or general base catalysis are more than 6 Å away from the scissile bond. However, in the 7A1-TSA structure (Figure 3C), the side chains of TyrL94 and TyrH50 reorient to form hydrogen bonds with the pro-*R* phosphonate oxygen of the TSA (Figure 6). All of these observations suggest that oxyanion stabilization plays a major role in the

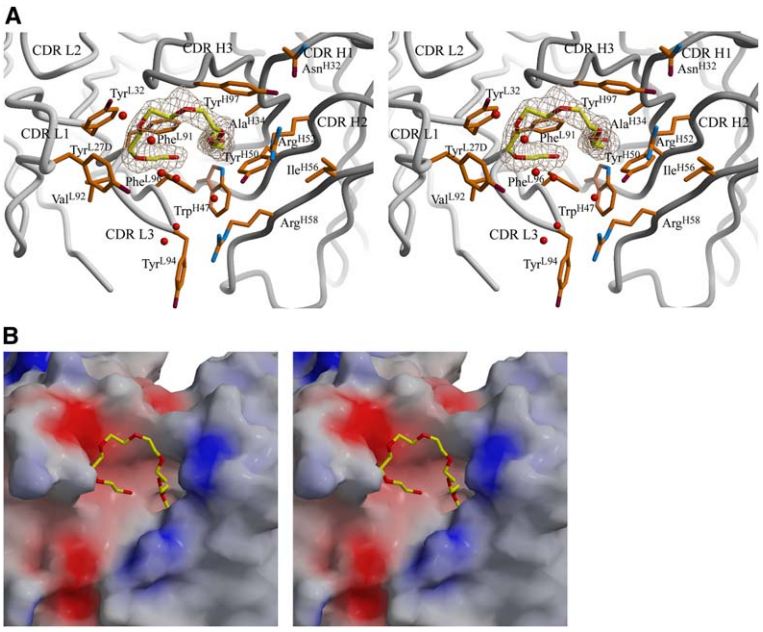

Figure 5. The Combining Site of the Antibody 7A1 in Complex with Heptaethylene Glycol

(A) Stereoview of the active site of 7A1 with bound heptaethylene glycol.

(B) Shape complementarity of heptaethylene glycol in the 7A1 combining site. The molecular surface is colored by electrostatic potential (calculated with GRASP [Nicholls et al., 1991] with a 1.4 Å probe radius and contoured between −30 to +30 kT).

catalysis, in which a solvent water molecule or hydroxide ion could attack the scissile carbonyl of the benzoyl ester and the antibody provides stabilization for the anionic transition state. Attack could be initiated from one side of the *re*- or *si*-face of the carbonyl group. Examination of the 7A1 crystal structures of the apo form, substrate, TSA, and product complexes (Figure 3) reveals that several water molecules are located in the active site, although none are positioned within contact distance (<3.9 Å away) of the pro-*R* or pro-*S* phosphonate oxygen atoms in the TSA complex, or of the scissile carbonyl in the cocaine complex. One conserved water

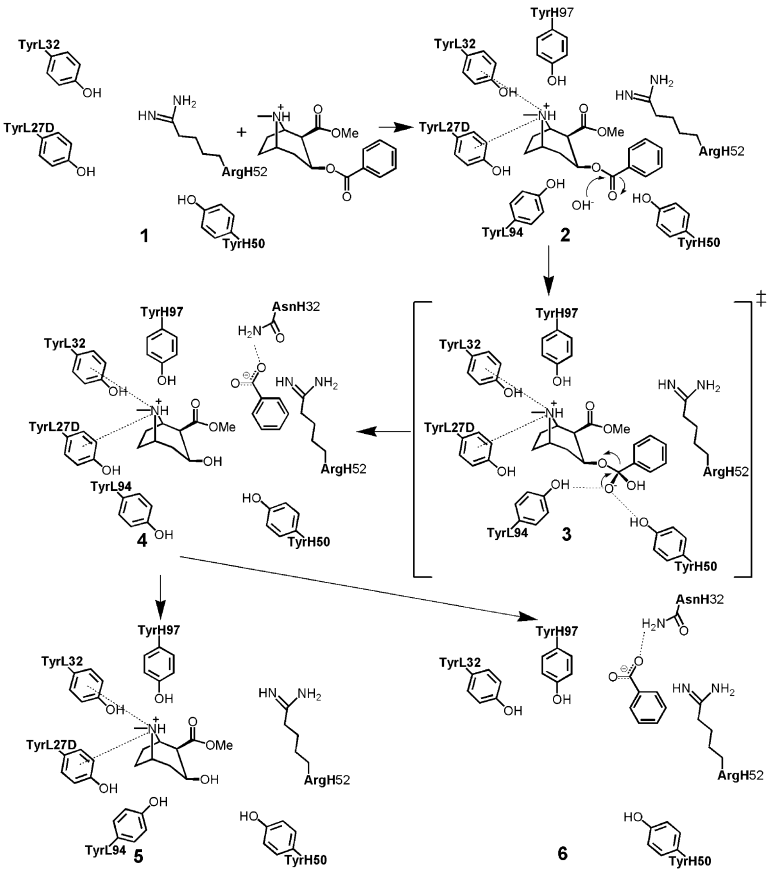

Figure 6. Proposed Mechanism for the 7A1-Catalyzed Cocaine Hydrolysis Reaction

The hydrogen bonds and cation-π interactions are shown in dotted lines (see the text for details). **1**, apo form; **2**, substrate bound state; **3**, transition state; **4**, two-product bound state; **5**, ecgonine methyl ester bound state; **6**, benzoic acid bound state. The flexible residues TyrL94, TyrH97 in **1**, and TyrL94 and TyrL27D in **6** are omitted.

molecule, S1, is buried deep within the active site pocket and hydrogen bonds to TrpH47 Nε1, except in the cocaine complex (Figure 3). This water molecule is 6–8 Å from the scissile carbonyl of cocaine or the phosphonate oxygen atoms of the TSA. However, analysis of the distribution of water molecules in the active sites of all of the structures shows some clustering on the *re*-face of cocaine on which TyrL94 and TyrH50 also reside. Furthermore, after superimposing the tropane-methyl ester moieties of the cocaine and TSA complexes, the benzoyl carbonyl oxygen of the cocaine almost overlaps with the pro-*S* oxygen of the TSA. Since the *si*-face around the benzoyl ester carbonyl group of the substrate cocaine is partially buried in the active site, all of these analyses indicate that the hydroxide ion could attack from the *re*-face. The intimate hydrogen bonds formed by TyrL94 (2.5 Å) and TyrH50 (2.6 Å) to the pro-*R* phosphonate oxygen of the transition state analog further suggest that these residues play an important role in stabilizing the developing negative charge on the transition state. In esterolytic antibody 7C8, only one tyrosine makes a hydrogen bond to its TSA (Gigant et al., 1997). In 7A1, the nucleophile must be a hydroxide ion or a water molecule, and TyrL94 and TyrH50 are hydrogen bond donors (Figure 6). The catalytic rate of 7A1 should then be a function of both hydroxide ion concentration and of the percentage of tyrosines that are in the protonated state. Once the hydrolytic reaction is achieved, both products would diffuse quickly into solvent, since no obvious product inhibition is observed in the kinetic experiments. Because the tropane and benzoic acid moieties are buried in such shallow slots in the combining site, each product of cocaine hydrolysis would no longer possess sufficient binding affinity to provide any observable product inhibition.

Comparison to Other Relevant Structures

To date, antibody 15A10 is the only other cocaine hydrolytic antibody with a reported crystal structure, although only in its apo form (Larsen et al., 2004). Comparison of antibody 7A1 with 15A10 reveals several significant differences. These two antibodies share only 33% identity in the light chain sequence and 44% identity in the heavy chain sequence (data not shown). At a structural level, the overall shape of the binding pocket of 15A10 is strikingly different from that of 7A1 due mainly to the different conformation of the CDR L3 and H3 loops, as well as the different side chain conformation of key residues; the binding pocket of 15A10 is also much deeper than that of 7A1. Although a crystal structure of 15A10 in complex with its TSA is not available, computational docking of a TSA into the published native crystal structure has led to a plausible binding model, which correlates well with results from site-directed mutagenesis and chemical modification (Larsen et al., 2004). The proposed model supports the notion that AsnH33, TyrH35, and TrpL96 donate four hydrogen bonds to the two phosphonate oxygens of the TSA to stabilize the transition state of the cocaine hydrolysis reaction. In antibody 7A1, TyrL94 and TyrH50 donate two hydrogen bonds to only one of the phosphonate oxygens of the TSA. Although there is no apparent electrostatic complementarity in the binding pocket of 15A10, two additional hydrogen bonds might contribute to stronger oxyanion stabilization and account for its higher rate enhancement (k_{cat} of 2.3 min^{-1}, K_M of 220 μM, and $k_{cat}k_{uncat}^{-1}$ of 23,000 measured in 50 mM PB at pH 7.8 [Yang et al., 1996]) compared to 7A1 (k_{cat} of 0.025 min^{-1}, K_M of 750 μM, and $k_{cat}k_{uncat}^{-1}$ of 2,630 measured in 100 mM PB at pH 7.4).

Crystal structures of seven other families of hydrolytic antibodies have been determined, including 17E8 (Zhou et al., 1994), CNJ206 (Charbonnier et al., 1995), D2.3 (Charbonnier et al., 1997), 48G7 (Wedemayer et al., 1997), 6D9 (Kristensen et al., 1998), 43C9 (Thayer et al., 1999), and MS6-12 (Ruzheinikov et al., 2003), which were raised against an aryl or benzyl phosphonate or phosphonamidate TSA and catalyze the hydrolysis of arylesters and amides. As summarized previously (Golinelli-Pimpaneau, 2002; Larsen et al., 2004), crystal structures of esterolytic catalytic antibodies have revealed obvious similarities in their TSA binding mode and in the oxyanion hole. Hydrogen bond-donating residues recognize the anionic phosphonate oxygens, and their aromatic moieties are sequestered in a hydrophobic pocket. In these antibodies, the hapten aryl group is buried deep within the binding pocket, which is not the case for the cocaine tropane skeleton in 7A1. Except for 6D9 and 7C8, the combining sites of the hydrolytic antibodies elicited against similar haptens also result in similar residues, such as HisH35, Tyr or Arg at L96, and residues at positions H100, H33, or H95, making more than three hydrogen bonds to the two oxygens of the hapten. For antibody 7A1, the hydrogen bond donors are two tyrosine residues, TyrH50 and TyrL94, which form two hydrogen bonds with only one of the hapten phosphonate oxygens. Based on our crystallographic analysis, site-directed mutagenesis of antibody 7A1 may now be carried out with a high degree of confidence to increase the number of hydrogen bonds with the transition state so as to stabilize the developing negative charge.

In conclusion, immunopharmacotherapy for cocaine addiction has been demonstrated to be a feasible treatment strategy for cocaine abuse. Cocaine degrades in vivo through modest hydrolysis and enzymatic degradation by liver carboxylesterase and serum butyrylcholinesterase; cocaine has an in vivo half-life of ~30 min. Hence, an effective cocaine catalytic antibody must out-compete these natural processes to diminish the psychoactive consequences of the drug. To achieve this goal of enzyme-like efficiency, it may be necessary to explore new approaches for eliciting and optimizing such catalytic activity. New functional groups could be introduced into the first-generation antibody catalysts by site-directed mutagenesis to circumvent the low probability of obtaining the required complex constellation of catalytic residues in a single step in the immunization process. An incremental approach will probably be required in which modest catalysts are improved by multiple rounds of mutagenesis and selection (MacBeath and Hilvert, 1996). These crystal structures of 7A1 now provide a foundation for antibody humanization and mutagenesis studies to enhance its cocaine catalytic activity. For 7A1, two key residues, TyrH50 and TyrL94, appear to stabilize the transition state, in contrast with other catalytic antibodies, such as CNJ206 and 17E8 (MacBeath and

Hilvert, 1996), in which positively charged residues stabilize the transition state. Replacement of TyrH50 and TyrL94 by lysine or arginine may improve catalytic activity. For 7A1, ArgH52, IleH56, ArgH58, and TyrH97 also undergo large conformational changes (up to 6 Å) in the catalytic process; thus, their relative contributions to catalysis should be further explored. An esterase antibody has been successfully evolved through selection of second shell residues, outside of the active site, which stabilize the active site structure (Arkin and Wells, 1998); hence, mutagenesis of second shell residues and screening by phage display could be another strategy (Arkin and Wells, 1998; Gao et al., 1997; Janda et al., 1997).

Structural dynamics are now included in the determination of the mechanism of action of many proteins. For enzymes, it is generally difficult to identify the key conformational changes in the reaction processes, as they are usually much faster than the chemical step and product release (Fersht, 1985). Conformational changes in antibodies have been examined by structural methods, but the available structural data have focused mainly on interactions with TSAs, which have confirmed the shape or chemical complementarity between the binding pocket and the haptenic TSA. The esterase-like antibody, D2.3, is the only other example for which crystal structures have been determined in complex with a substrate analog, TSA, or one of the reaction products. However, in this case, significant structural differences were not observed along the reaction pathway (Gigant et al., 1997), although extensive kinetic studies suggested the importance of conformational changes (Lindner et al., 1999). Thus, this comprehensive study of high-resolution crystal structures of antibody 7A1, in the apo form, substrate complex, TSA complex, and products complexes, have shed light on the sequence of events from substrate to products in an antibody-mediated reaction, and it provides a rare snapshot of structural dynamics that can occur in antibody and enzyme catalysis.

Experimental Procedures

Kinetic and Inhibition Measurements

Murine monoclonal antibody 7A1 was elicited against hapten GNL **5** (Figure 1) coupled to keyhole limpet hemocyanin (KLH) as previously described (Matsushita et al., 2001). The initial rates of 7A1-catalyzed degradation of cocaine were determined by monitoring the formation of benzoic acid by analytical reversed-phase HPLC (RP-HPLC) and were quantified at 254 nm (Hitachi L-7200; Vydac 201TP54 C-18 column; isocratic mobile phase of 17% MeCN, 83% H_2O [0.1% TFA]; flow rate 1 ml/min). The retention times for benzoic acid, benzoylecgonine, and cocaine were 10 min, 7.5 min, and 13 min, respectively. Benzoic acid concentrations were determined by interpolation of peak height and area values relative to standard curves. Unless otherwise noted, all reactions were performed in 100 mM MOPS (pH 7.4), and all of the experiments were performed in triplicate.

The dependence of the cocaine hydrolysis rate on pH was determined by the measurement of the V_{max} of 7A1 in 100 mM MOPS at pH 6.4, 7.1, 7.4, 8.0, and 8.5. In all cases, reactions were prepared by mixing antibody (20 μM) and cocaine (2.8 mM) at 23ºC. Every 200 min, an aliquot was removed from the reactions and analyzed by RP-HPLC by using the described separation conditions.

For the study of the inhibition of 7A1 by ecgonine methyl ester, a solution was prepared containing antibody (20 μM), cocaine (0.5–4.0 mM), and ecgonine methyl ester (0–3.7 mM). After several hours of incubation at 23ºC, an aliquot was removed and analyzed for benzoic acid formation by RP-HPLC by using the described separation conditions. In order to assess the inhibition of 7A1 by benzoic acid or heptaethylene glycol, reactions were prepared containing antibody (20 μM), cocaine (2.8 mM), and benzoic acid or heptaethylene glycol (1 mM). The rate of benzoic acid formation was compared to that of control reactions containing antibody (20 μM) and cocaine (2.8 mM) alone. Further control samples containing benzoic acid (100 μM–10 mM) were also analyzed. In all cases, after several hours of incubation, an aliquot was removed and analyzed by RP-HPLC by using the described separation conditions.

Fab′ Preparation and Purification

The Fab′ fragment of 7A1 was produced by standard protocols (Harlow and Lane, 1998). The intact 7A1 IgG was digested to $(Fab')_2$ with 2% (w/w) pepsin for 4 hr and was followed by reduction to Fab′ by 20 mM 2-mercaptoethylamine (MEA) for 4 hr. The protein was purified to homogeneity by a combination of protein A and protein G affinity chromatography, as well as by ion-exchange chromatography (Mono-Q column, Pharmacia) and gel filtration (Super-200 column, Pharmacia).

Crystallization Conditions

7A1 Fab′ was concentrated to 10.7 mg/ml in 0.1 M sodium acetate (pH 5.5). Crystallization experiments were performed by using the sitting-drop, vapor diffusion method at 295K (1 μl reservoir solution and 1 μl protein solution). Apo crystals were grown from 0.1 M sodium acetate (pH 5.5), 0.2 M ammonium sulfate, 9.5 mM flavin adenine dinucleotide (FAD), and 20% (w/v) polyethylene glycol (PEG) 4000. For the substrate cocaine complex, 7A1 Fab′ was mixed with 7.7 mM cocaine-HCl immediately prior to crystallization from 0.1 M sodium acetate (pH 5.5), 0.2 M ammonium formate, and 20% (w/v) PEG 4000. 7A1 Fab′ and TSA were cocrystallized from 0.1 M sodium acetate (pH 5.5), 0.2 M ammonium fluoride, and 20% (w/v) PEG 4000 with 5.0 mM TSA. 7A1 Fab′ was incubated with 3.8 mM ecgonine methyl ester, 3.8 mM benzoic acid, and the two-product cocrystals were grown from 0.1 M sodium acetate (pH 5.5), 0.2 M zinc acetate, and 20% (w/v) PEG 4000. 7A1 Fab′ and the product ecgonine methyl ester were cocrystallized from 0.1 M sodium acetate (pH 5.5), 0.2 M ammonium fluoride, and 20% (w/v) PEG 4000 with 7.7 mM ecgonine methyl ester. 7A1 Fab′ was incubated with 25 mM benzoic acid, and the product benzoic acid cocrystals were grown from 0.1 M sodium acetate (pH 5.5), 0.2 M zinc acetate, and 20% (w/v) PEG 4000. 7A1 Fab′ and heptaethylene glycol cocrystals arose from 0.1 M HEPES (pH 7.5), 2% (w/v) PEG 4000, and 2.0 M ammonium sulfate.

Data Collection and Processing

Crystals of apo 7A1 Fab′ and its other complexes were flash-cooled in liquid nitrogen with 20%–25% (v/v) glycerol as cryoprotectant. Data sets were collected at the Advance Light Source (ALS) beamline 8.3.1 (ADSC Quantum 210 CCD detector) for the apo form 7A1 Fab′ and its complex with ecgonine methyl ester and benzoic acid, at ALS beamline 8.2.1 (ADSC Quantum 210 CCD detector) for the cocaine complex, at ALS beamline 5.0.2 (ADSC Quantum 210 CCD detector) for the TSA complex and the ecgonine methyl ester complex, at ALS beamline 8.2.2 (ADSC Quantum 315 CCD detector) for the benzoic acid complex, and at the Stanford Synchrotron Radiation Laboratory (SSRL) beamline 9-2 (ADSC Quantum 4 CCD detector) for the heptaethylene glycol complex. All of the data sets were integrated and scaled with HKL2000 (Otwinowski and Minor, 1997) (see Table 2).

Structure Determination and Refinement

The 7A1 Fab′-heptaethylene glycol structure was determined by molecular replacement with the program AMoRe (Navaza, 1994) and Fab A5B7 (PDB code: 1CLO) as a search model. The refined structure was then used for molecular replacement of all other data sets. Structural refinement of the apo, cocaine, and heptaethylene glycol Fab′ structures was initiated in CNS (Brünger et al., 1998) and completed with REFMAC5 (Murshudov et al., 1999). Anisotropic B value refinement and alternate conformations for some side chains were implemented for the apo and cocaine complexes. The TSA complex and all product complexes were refined in CNS (Brünger

et al., 1998). NCS restraints of 400 kcal/mol and 200 kcal/mol for main chain and side chain side atoms, respectively, were applied to the initial refinement of the two-product complex. All ligands were initially constructed and energy minimized by using InsightII (ACCELRYS, San Diego, CA). Hydrogen bonds were evaluated with HBPLUS (McDonald and Thornton, 1994) and CONTACTSYM (Sheriff et al., 1987), and the electrostatic surface was evaluated with GRASP (Nicholls et al., 1991). The approximate volume of the combining site was calculated from the manually scribed molecular surface in GRASP (Nicholls et al., 1991). Shape complementarity between antibody and ligands was evaluated by the Sc parameter calculated with the program SC (Lawrence and Colman, 1993).

Acknowledgments

We thank the staffs of the Advanced Light Source and the Stanford Synchrotron Radiation Laboratory, Xiaoping Dai for assistance on synchrotron trips, Robyn Stanfield for helpful discussions, and Sharon Ferguson for excellent assistance with antibody digestion. Support was provided by the National Institutes of Health grants GM38273 (I.A.W.) and DA08590 and DA15700 (K.D.J.), and by The Skaggs Institute for Chemical Biology, The Scripps Research Institute (I.A.W. and K.D.J.). This paper is manuscript no. 17605-MB of The Scripps Research Institute.

Received: August 17, 2005
Revised: September 27, 2005
Accepted: October 4, 2005
Published: February 10, 2006

References

Al-Lazikani, B., Lesk, A.M., and Chothia, C. (1997). Standard conformations for the canonical structures of immunoglobulins. J. Mol. Biol. *273*, 927–948.

Allen, F.H. (2002). The Cambridge Structural Database: a quarter of a million crystal structures and rising. Acta Crystallogr. B *58*, 380–388.

Arkin, M.R., and Wells, J.A. (1998). Probing the importance of second sphere residues in an esterolytic antibody by phage display. J. Mol. Biol. *284*, 1083–1094.

Brünger, A.T., Adams, P.D., Clore, G.M., DeLano, W.L., Gros, P., Grosse-Kunstleve, R.W., Jiang, J.S., Kuszewski, J., Nilges, M., Pannu, N.S., et al. (1998). Crystallography & NMR system: a new software suite for macromolecular structure determination. Acta Crystallogr. D Biol. Crystallogr. *54*, 905–921.

Carrera, M.R., Ashley, J.A., Parsons, L.H., Wirsching, P., Koob, G.F., and Janda, K.D. (1995). Suppression of psychoactive effects of cocaine by active immunization. Nature *378*, 727–730.

Carrera, M.R., Ashley, J.A., Zhou, B., Wirsching, P., Koob, G.F., Janda, K.D., and Parsons, L.H. (2000). Cocaine vaccines: antibody protection against relapse in a rat model. Proc. Natl. Acad. Sci. USA *97*, 6202–6206.

Charbonnier, J.B., Carpenter, E., Gigant, B., Golinelli-Pimpaneau, B., Eshhar, Z., Green, B.S., and Knossow, M. (1995). Crystal structure of the complex of a catalytic antibody Fab fragment with a transition state analog: structural similarities in esterase-like catalytic antibodies. Proc. Natl. Acad. Sci. USA *92*, 11721–11725.

Charbonnier, J.B., Golinelli-Pimpaneau, B., Gigant, B., Tawfik, D.S., Chap, R., Schindler, D.G., Kim, S.H., Green, B.S., Eshhar, Z., and Knossow, M. (1997). Structural convergence in the active sites of a family of catalytic antibodies. Science *275*, 1140–1142.

Dougherty, D.A. (1996). Cation-π interactions in chemistry and biology: a new view of benzene, Phe, Tyr, and Trp. Science *271*, 163–168.

Esnouf, R.M. (1999). Further additions to MolScript version 1.4, including reading and contouring of electron-density maps. Acta Crystallogr. D Biol. Crystallogr. *55*, 938–940.

Fersht, A.R. (1985). Enzyme Structure and Mechanism (New York: W.H. Freeman).

Fox, B.S., Kantak, K.M., Edwards, M.A., Black, K.M., Bollinger, B.K., Botka, A.J., French, T.L., Thompson, T.L., Schad, V.C., Greenstein, J.L., et al. (1996). Efficacy of a therapeutic cocaine vaccine in rodent models. Nat. Med. *2*, 1129–1132.

Gao, C., Lin, C.H., Lo, C.H., Mao, S., Wirsching, P., Lerner, R.A., and Janda, K.D. (1997). Making chemistry selectable by linking it to infectivity. Proc. Natl. Acad. Sci. USA *94*, 11777–11782.

Gigant, B., Charbonnier, J.B., Eshhar, Z., Green, B.S., and Knossow, M. (1997). X-ray structures of a hydrolytic antibody and of complexes elucidate catalytic pathway from substrate binding and transition state stabilization through water attack and product release. Proc. Natl. Acad. Sci. USA *94*, 7857–7861.

Golinelli-Pimpaneau, B. (2002). Structural diversity of antibody catalysts. J. Immunol. Methods *269*, 157–171.

Gutteridge, A., and Thornton, J. (2004). Conformational change in substrate binding, catalysis and product release: an open and shut case? FEBS Lett. *567*, 67–73.

Harlow, K.U., and Lane, D. (1998). Antibodies: A Laboratory Manual (Cold Spring Harbor, NY: Cold Spring Harbor Press).

Janda, K.D., Lo, L.C., Lo, C.H., Sim, M.M., Wang, R., Wong, C.H., and Lerner, R.A. (1997). Chemical selection for catalysis in combinatorial antibody libraries. Science *275*, 945–948.

Koshland, D.E., Jr. (1998). Conformational changes: how small is big enough? Nat. Med. *4*, 1112–1114.

Kristensen, O., Vassylyev, D.G., Tanaka, F., Morikawa, K., and Fujii, I. (1998). A structural basis for transition-state stabilization in antibody-catalyzed hydrolysis: crystal structures of an abzyme at 1.8 Å resolution. J. Mol. Biol. *281*, 501–511.

Larsen, N.A., Zhou, B., Heine, A., Wirsching, P., Janda, K.D., and Wilson, I.A. (2001). Crystal structure of a cocaine-binding antibody. J. Mol. Biol. *311*, 9–15.

Larsen, N.A., de Prada, P., Deng, S.X., Mittal, A., Braskett, M., Zhu, X., Wilson, I.A., and Landry, D.W. (2004). Crystallographic and biochemical analysis of cocaine-degrading antibody 15A10. Biochemistry *43*, 8067–8076.

Lawrence, M.C., and Colman, P.M. (1993). Shape complementarity at protein/protein interfaces. J. Mol. Biol. *234*, 946–950.

Lindner, A.B., Eshhar, Z., and Tawfik, D.S. (1999). Conformational changes affect binding and catalysis by ester-hydrolysing antibodies. J. Mol. Biol. *285*, 421–430.

MacBeath, G., and Hilvert, D. (1996). Hydrolytic antibodies: variations on a theme. Chem. Biol. *3*, 433–445.

Matsushita, M., Hoffman, T.Z., Ashley, J.A., Zhou, B., Wirsching, P., and Janda, K.D. (2001). Cocaine catalytic antibodies: the primary importance of linker effects. Bioorg. Med. Chem. Lett. *11*, 87–90.

McDonald, I.K., and Thornton, J.M. (1994). Satisfying hydrogen bonding potential in proteins. J. Mol. Biol. *238*, 777–793.

Merritt, E.A., and Murphy, M.E.P. (1994). Raster3d version 2.0 - a program for photorealistic molecular graphics. Acta Crystallogr. D Biol. Crystallogr. *50*, 869–873.

Morea, V., Tramontano, A., Rustici, M., Chothia, C., and Lesk, A.M. (1998). Conformations of the third hypervariable region in the V_H domain of immunoglobulins. J. Mol. Biol. *275*, 269–294.

Murshudov, G.N., Vagin, A.A., Lebedev, A., Wilson, K.S., and Dodson, E.J. (1999). Efficient anisotropic refinement of macromolecular structures using FFT. Acta Crystallogr. D Biol. Crystallogr. *55*, 247–255.

Navaza, J. (1994). Amore - an automated package for molecular replacement. Acta Crystallogr. A *50*, 157–163.

Nicholls, A., Sharp, K.A., and Honig, B. (1991). Protein folding and association: insights from the interfacial and thermodynamic properties of hydrocarbons. Proteins *11*, 281–296.

Otwinowski, Z., and Minor, W. (1997). Processing of X-ray diffraction data collected in oscillation mode. Methods Enzymol. *276*, 307–326.

Pozharski, E., Moulin, A., Hewagama, A., Shanafelt, A.B., Petsko, G.A., and Ringe, D. (2005). Diversity in hapten recognition: structural study of an anti-cocaine antibody M82G2. J. Mol. Biol. *349*, 570–582.

Ruzheinikov, S.N., Muranova, T.A., Sedelnikova, S.E., Partridge, L.J., Blackburn, G.M., Murray, I.A., Kakinuma, H., Takahashi-Ando,

N., Shimazaki, K., Sun, J., et al. (2003). High-resolution crystal structure of the Fab-fragments of a family of mouse catalytic antibodies with esterase activity. J. Mol. Biol. *332*, 423–435.

SAMHSA (Substance Abuse and Mental Health Services and Administration). (2004). Results from the 2003 National Survey on Drug Use and Health: National Findings. (Office of Applied Studies, NSDUH Series H-25, DHHS Publication No. SMA 04–3964). Rockville, MD).

Sheriff, S., Hendrickson, W.A., and Smith, J.L. (1987). Structure of myohemerythrin in the azidomet state at 1.7/1.3 Å resolution. J. Mol. Biol. *197*, 273–296.

Sofuoglu, M., and Kosten, T.R. (2005). Novel approaches to the treatment of cocaine addiction. CNS Drugs *19*, 13–25.

Tanaka, F. (2002). Catalytic antibodies as designer proteases and esterases. Chem. Rev. *102*, 4885–4906.

Thayer, M.M., Olender, E.H., Arvai, A.S., Koike, C.K., Canestrelli, I.L., Stewart, J.D., Benkovic, S.J., Getzoff, E.D., and Roberts, V.A. (1999). Structural basis for amide hydrolysis catalyzed by the 43C9 antibody. J. Mol. Biol. *291*, 329–345.

Wedemayer, G.J., Patten, P.A., Wang, L.H., Schultz, P.G., and Stevens, R.C. (1997). Structural insights into the evolution of an antibody combining site. Science *276*, 1665–1669.

Wilson, I.A., and Stanfield, R.L. (1993). Antibody-antigen interactions. Curr. Opin. Struct. Biol. *3*, 113–118.

Yang, G., Chun, J., Arakawa-Uramoto, H., Wang, X., Gawinowicz, M.A., Zhao, K., and Landry, D.W. (1996). Anti-cocaine catalytic antibodies: A synthetic approach to improved antibody diversity. J. Am. Chem. Soc. *118*, 5881–5890.

Zhan, C.G., and Landry, D.W. (2001). Theoretical studies of competing reaction pathways and energy barriers for alkaline ester hydrolysis of cocaine. J. Phys. Chem. A *105*, 1296–1301.

Zhou, G.W., Guo, J., Huang, W., Fletterick, R.J., and Scanlan, T.S. (1994). Crystal structure of a catalytic antibody with a serine protease active site. Science *265*, 1059–1064.

Zhu, X., Heine, A., Monnat, F., Houk, K.N., Janda, K.D., and Wilson, I.A. (2003). Structural basis for antibody catalysis of a cationic cyclization reaction. J. Mol. Biol. *329*, 69–83.

Accession Numbers

Atomic coordinates and structure factors have been deposited in the Protein Data Bank with accession codes: 2aju, 7A1 Fab′ in the apo form; 2ajv, cocaine complex; 2ajx, TSA complex; 2ajy, two-product complex; 2ajz, ecgonine methyl ester complex; 2ak1, benzoic acid complex; 2ajs, heptaethylene glycol complex.